ADVANCED MATERIALS
www.advmat.de

Deep-Red Perovskite Light-Emitting Diodes Based on One-Step-Formed γ-$CsPbI_3$ Cuboid Crystallites

*Yanfeng Miao, Xiaomin Liu, Yuetian Chen, Taiyang Zhang, Tianfu Wang, and Yixin Zhao**

Inorganic $CsPbI_3$ perovskite with high chemical stability is attractive for efficient deep-red perovskite light-emitting diodes (PeLEDs) with high color purity. Compared to PeLEDs based on ex-situ-synthesized $CsPbI_3$ nanocrystals/quantum dots suffering from low conductivity and efficiency droop under high current densities, in situ deposited 3D $CsPbI_3$ films from precursor solutions can maintain high conductivity but show high trap density. Here, it is demonstrated that introducing diammonium iodide can increase the size of colloids in the precursor solution, retard the phase-transition rate, and passivate trap states of the in-situ-formed cuboid crystallites. The PeLED based on the one-step-formed 3D $CsPbI_3$ cuboid crystallite films shows a peak external quantum efficiency (EQE) value up to 15.03% because of the high conductivity and reduced trap states. Furthermore, this one-step method also has a wide processing window, which is attractive for flow-line production of large-area PeLED modules. The fabrication of a 9 cm^2 PeLED that exhibits a peak EQE of 10.30% is successfully demonstrated.

1. Introduction

Other than the well-known application as perovskite solar cells, metal halide perovskites are also promising for efficient light-emitting diodes because of their high charge carrier mobility and high photoluminescence quantum yield (PLQY).[1–6] The record EQE of PeLEDs has reached to more than 23% over the past several years, showing potential for next-generation solid-state lightings and displays.[7–15] Despite unprecedented efficiency progress, the stability and brightness of PeLEDs are still limited, especially for PeLEDs with visible-light emission.[16–20]

Compared to organic–inorganic perovskites based on volatile organic cations, inorganic $CsPbI_3$ perovskite emitting red light is more attractive for chemically stable PeLEDs.[19,21,22] The main problem for realizing efficient $CsPbI_3$ PeLED is the phase degradation of $CsPbI_3$ from black phase (α-phase, β-phase, and γ-phase) to yellow non-perovskite phase (δ-phase) at room temperature.[23,24] Currently, most of the reported $CsPbI_3$ PeLEDs are based on $CsPbI_3$ nanocrystals/quantum dots because the ligand-covered nanocrystal surface can passivate surface defects and stabilize black phase $CsPbI_3$. Some spacer cations such as 1-naphthylmethylammonium and phenylbutylammonium can facilitate the formation of quasi-2D perovskite with smooth surface and improved PLQY.[21,25] However, The long-chained ligands of QDs and organic spacer layers of quasi-2D perovskites will resist the charge injection to PeLEDs and cause EQE roll-off under high current density and high brightness.[26–29]

Alternatively, bulk 3D $CsPbI_3$ films without long chain ligands, which often obtained from spin-coating the precursor solutions directly, can maintain the high conductivity of $CsPbI_3$ perovskite.[19,21,25,30,31] Organic cations such as dimethylammonium (DMA^+), methylammonium (MA^+), and imidazolium (IZ^+) have been found to form an intermediate phase which will reduce the activation energy for phase transition to black phase 3D $CsPbI_3$.[19,32,33] However, 3D $CsPbI_3$ films still suffer from high trap densities that will cause serious nonradiative recombination and reduce the efficiency and operation stability of PeLEDs.[31,34]

In this work, we report a one-step method to in situ deposit γ-phase 3D $CsPbI_3$ perovskite films consisting of $CsPbI_3$ cuboid crystallites, which is achieved by introducing diammonium-cation-based 1,3-propanediamine dihydriodide (PDAI). The obtained perovskite is noted as PDAI-$CsPbI_3$. The addition of PDAI can slow down the phase transition from intermediate phase to γ-phase $CsPbI_3$ and increase the size of cuboid crystallites. Meanwhile, the PDAI residue covering the surface of the final films can passivate defects and improve their PLQYs. Consequently, the PeLED based on such PDAI-$CsPbI_3$ film can reach a champion peak EQE of 15.03% and deep-red emission with high color purity. The T_{50} lifetime (time to half of the initial brightness) can reach to 1.7 h under a high current density of 100 mA cm^{-2}. This PDAI-assisted one-step method also has a wide processing window. The large-area PDAI-$CsPbI_3$-based PeLED we fabricated with active area of 9 cm^2 can reach a peak EQE of 10.30%.

2. Results and Discussion

PDAI-$CsPbI_3$ perovskite films were prepared by spin-coating a precursor solution of formamidinium iodide (FAI), CsI, PDAI,

Y. Miao, X. Liu, Y. Chen, T. Zhang, T. Wang, Y. Zhao
School of Environmental Science and Engineering
Frontiers Science Center for Transformative Molecules
Shanghai Jiao Tong University
Shanghai 200240, China
E-mail: yixin.zhao@sjtu.edu.cn

The ORCID identification number(s) for the author(s) of this article can be found under https://doi.org/10.1002/adma.202105699.

DOI: 10.1002/adma.202105699

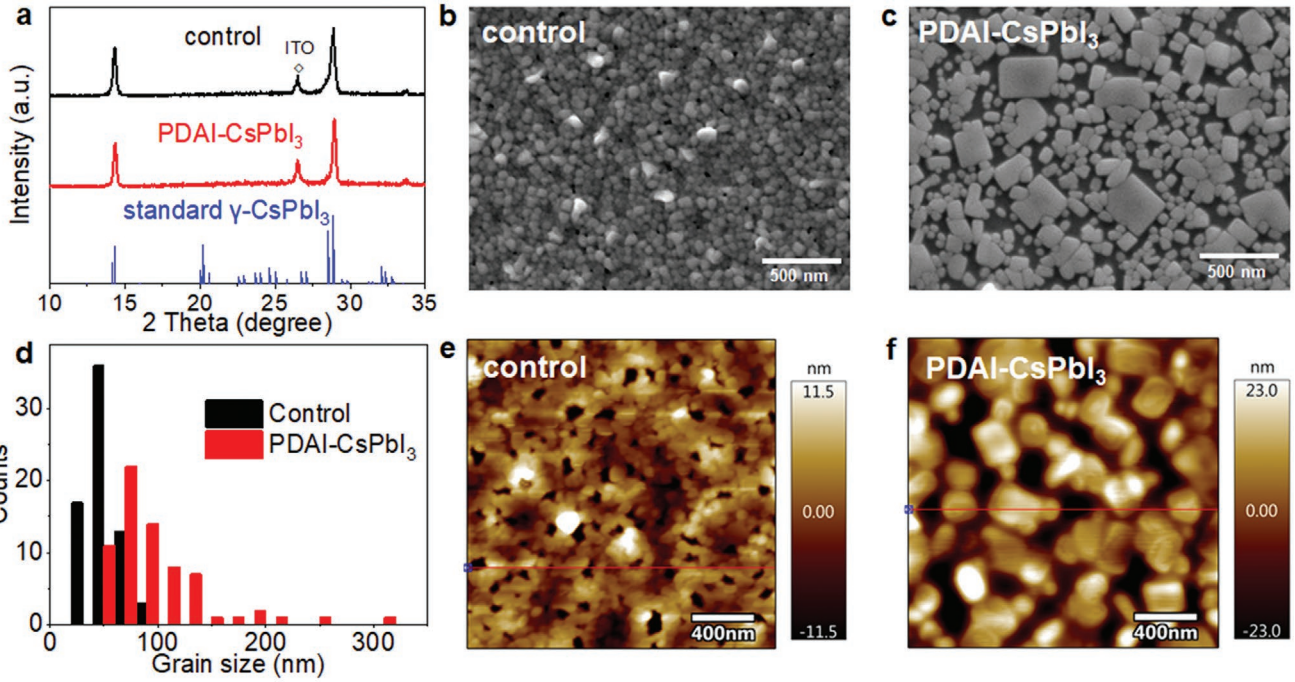

Figure 1. Characterizations of the control and PDAI-$CsPbI_3$ films. a) XRD patterns of the control film, PDAI-$CsPbI_3$ film, and standard γ-$CsPbI_3$. b,c) SEM images for the control film and PDAI-$CsPbI_3$ film. d) Statistics of grain sizes for the control film and PDAI-$CsPbI_3$ film. e,f) AFM images for the control film and PDAI-$CsPbI_3$ film.

and PbI_2 with a molar ratio of 1:1.5:*x*:1 dissolved in *N*,*N*-dimethylformamide (DMF) and then annealed at 100 °C for 10 min. $x = 0$ is defined as the control film; the noted PDAI-$CsPbI_3$ film is the optimal sample with $x = 0.5$. In this method, FAI in the precursor is supposed to work as additive to help the crystallization of black phase $CsPbI_3$ perovskite.[33,35] X-ray diffraction (XRD) patterns of the control and PDAI-$CsPbI_3$ films have two significant diffraction peaks at 14.3° and 28.9°, representing the (110) and (220) reflections of the γ-phase $CsPbI_3$, respectively (**Figure 1**a).[36] This result confirms the formation of black-phase $CsPbI_3$ perovskite with the help of FAI additive, which is consistent with previous reports.[33,37,38] Scanning electron microscopy (SEM) images show that PDAI additive will change the morphology from small grains with size of ≈50 nm to rectangular-shape crystals with sizes ranging from 50 to 350 nm (Figure 1b–d). SEM images also show that PDAI-$CsPbI_3$ film has lower film coverage than the control film. However, such low coverage will not influence the charge carrier injection in PeLEDs as discussed in the next section.

Atomic force microscopy (AFM) images have similar topology with the SEM images (Figure 1e,f). AFM line scans show that grains of PDAI-$CsPbI_3$ film are flatter on surfaces (Figure S1a,b, Supporting Information), which indicated that PDAI would induce the formation of $CsPbI_3$ cuboid crystallites. Cross-section SEM image also proved that those perovskite cuboid crystallites are more homogeneous and smoother (Figure S1c, Supporting Information).

To explore the effect of PDAI additive, we started from investigating the chemical profiles of the precursor solution by proton nuclear magnetic resonance (^{1}H-NMR) and dynamic light scattering (DLS). The ^{1}H-NMR spectra in **Figure 2**a show that FAI exhibits two peaks at 7.90 and 8.82 ppm, and PDAI has three peaks at 1.83, 2.91, and 7.74 ppm. The addition of FAI into the mixed precursor solution of PbI_2 and CsI will not greatly alter the peak position of protons in FAI. In the precursor solution with PDAI, FAI, PbI_2, and CsI, the main peaks are 1.83 and 2.91 ppm from PDAI with only one strong peak of 7.90 ppm from FAI, which means that PDAI will have strong interactions with FAI in the precursor solution.[17,39,40] DLS measurement shows that the average colloid sizes of the control precursor solution and PDAI-$CsPbI_3$ precursor solution are 793 and 1226 nm, respectively (Figure 2b). The increase of colloid size could be ascribed to the interaction between PDAI and FAI in the precursor solution. We hypothesize that PDAI with two ammonium groups may crosslink the neighboring colloids and improve overall colloid size in precursor solution, which leads to an increment to the final film's crystal grain size.

To further explore the effect of PDAI over the film formation process, we first prepared precursor films without annealing by just spin-coating the precursor solution. The effect of PDAI in precursor films is studied by X-ray photoelectron spectroscopy (XPS) and XRD. The XPS spectra of the control precursor film and PDAI-$CsPbI_3$ precursor film (Figure 2c) indicated that the core level of Pb $4f_{7/2}$ and Pb $4f_{5/2}$ has shifted to higher binding energy for PDAI-$CsPbI_3$ precursor film. This result means that PDAI has strong bonding with Pb^{2+} in the precursor film, and this effect could retard the phase transition rate during annealing. We compared the phase transformation rate of the control film and PDAI-$CsPbI_3$ film. The XRD patterns and photograph at different annealing times (Figures S2 and S3, Supporting Information) show that the control film has black phase $CsPbI_3$ at 0.5 min, while the PDAI-$CsPbI_3$ film still maintain

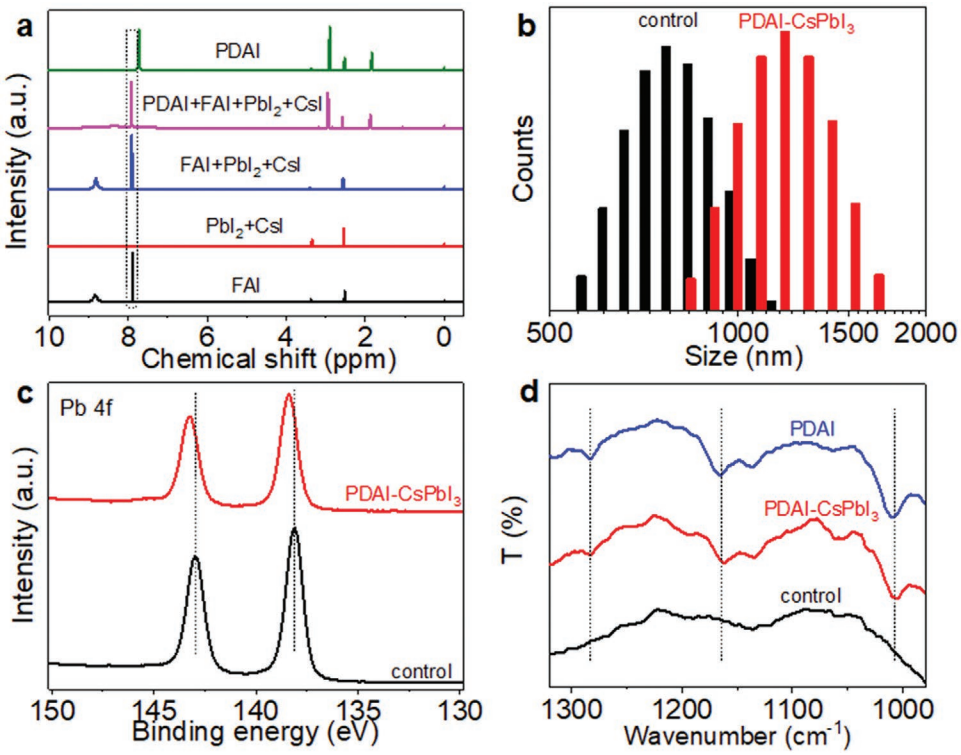

Figure 2. Characterizations of precursor solutions, precursor films, and perovskite films. a) ^{1}HNMR spectra of FAI, PbI_2+CsI, FAI+PbI_2+CsI, PDAI+FAI+PbI_2+CsI, and PDAI precursor solutions. b) Colloid size of the control and PDAI-$CsPbI_3$ precursor solutions. c) XPS spectra of the control and PDAI-$CsPbI_3$ precursor films. d) FTIR spectra of PDAI film, PDAI-$CsPbI_3$ film, and the control film.

the amorphous intermediate phase, which confirmed that PDAI retarded the phase transition. We believe that the interaction between PDAI and FAI/PbI_2 contributes to the formation of a stable intermediate. This stable intermediate will reduce phase transition rate, help with the formation of $CsPbI_3$ cuboid crystallites, and improve their crystal quality.[41] Recently, works from Zhu et al. and Zou et al. also reported that the interaction between additive and FAI/PbI_2 will form stable intermediate and retard perovskite nucleation, yielding high-quality crystallites with reduced trap densities.[42,43] These conclusions agree well with our experimental results.

We further prepared perovskite films with different PDAI:PbI_2 molar ratios to investigate how the concentration of PDAI influences the crystal growth. SEM images (Figure S4a–d, Supporting Information) show that 0.25 PDAI can significantly improve the grain size but these grains have irregular shape. 0.5 PDAI can further control the nucleation process and have faceted crystallites. When PDAI increased to 0.75, the film exhibits small crystallites because high concentration of organic additives will impede the crystal growth.[6] XRD patterns also show reduced peak intensity for 0.75 PDAI (Figure S4e, Supporting Information). The high crystal quality of 0.5 PDAI film correlated well with the highest PLQY among different PDAI concentrations (Figure S4f, Supporting Information).

Fourier transform infrared (FTIR) spectroscopy was measured to confirm whether PDA is left on the final film after annealing. FTIR spectra (Figure 2d) show that the PDAI-$CsPbI_3$ film has three characteristic signals from ν_{C-N} of PDA in the range of 1300 to 1000 cm^{-1}, which confirmed the existence of PDA in the final film. To better understand the chemical composition of the final perovskite film, we further characterized the elemental and group distribution of PDAI-$CsPbI_3$ film by time-of-flight secondary-ion mass spectrometry (ToF-SIMS). The depth profile in **Figure 3**a shows that Cs, Pb, and I distributed uniformly across the entire film while the amount of PDA reduced rapidly from the top surface to bottom. 3D profile of PDA group shows that PDA mainly located on the surface of the film (Figure 3b).

As shown in Figure 3c, PL and absorption spectra indicated that the peak position of PDAI-$CsPbI_3$ film redshifted compared with the control film. This redshift can be attributed to the increased grain size and reduced quantum confinement effect.[44] PDAI-$CsPbI_3$ film has stronger PL intensity than the control film. Compared to the control film, the light intensity-dependent PLQYs of PDAI-$CsPbI_3$ film were greatly enhanced, indicating reduced trap states and inhibited nonradiative recombination (Figure S5, Supporting Information). Time-resolved photoluminescence (TRPL) revealed that PDAI-$CsPbI_3$ film has significantly longer PL lifetime than the control film, which may benefit from the synergistic effect of both improved crystal size and reduced trap density of the PDAI-$CsPbI_3$ film (Figure 3d).

We fabricated PeLEDs with a device configuration of indium tin oxide (ITO)/polyethylenimine ethoxylated (PEIE)-modified zinc oxide (ZnO, 30 nm)/perovskite/poly(9,9-dioctyl-fluorene-*co*-*N*-(4-butylphenyl)diphenylamine) (TFB, 40 nm)/molybdenum oxide (MoOx, 7 nm)/silver (Ag, 60 nm) (**Figure 4**a). PeLED based on the control film only reached a peak EQE of

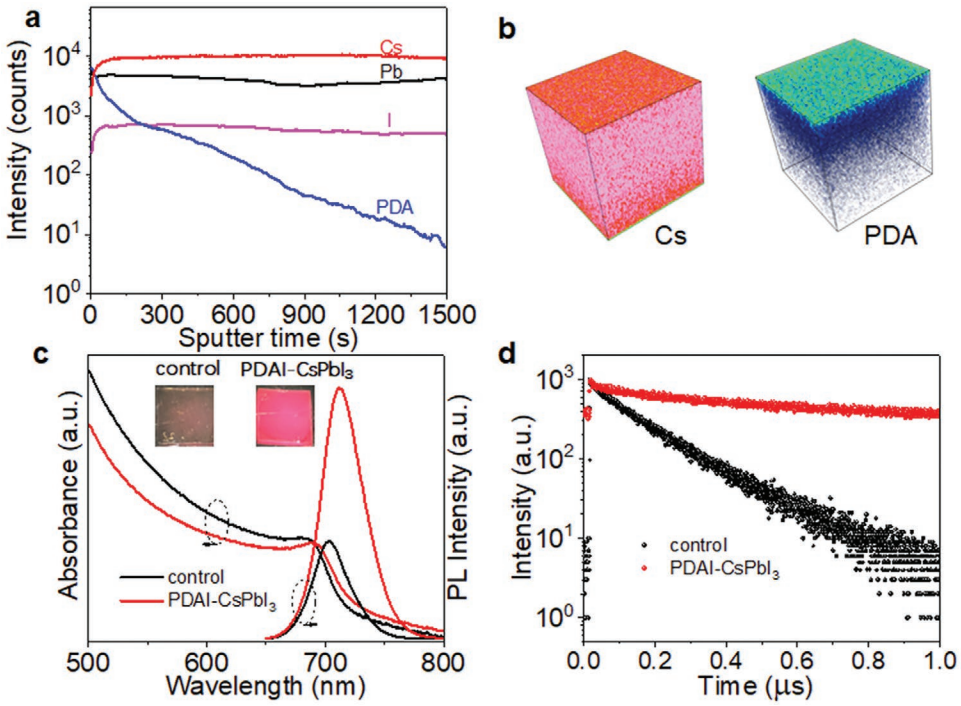

Figure 3. Element distribution and optoelectronic properties of the control and PDAI-$CsPbI_3$ films. a) ToF-SIMS depth profiles for Cs, Pb, I, and PDA in PDAI-$CsPbI_3$ film. b) 3D element and group distributions for Cs and PDA in PDAI-$CsPbI_3$ film. c) PL spectra and UV–vis absorption spectra for the control film and PDAI-$CsPbI_3$ film. Images inset: photographs of the control film and PDAI-$CsPbI_3$ film under UV light (365 nm). d) TRPL for the control film and PDAI-$CsPbI_3$ film.

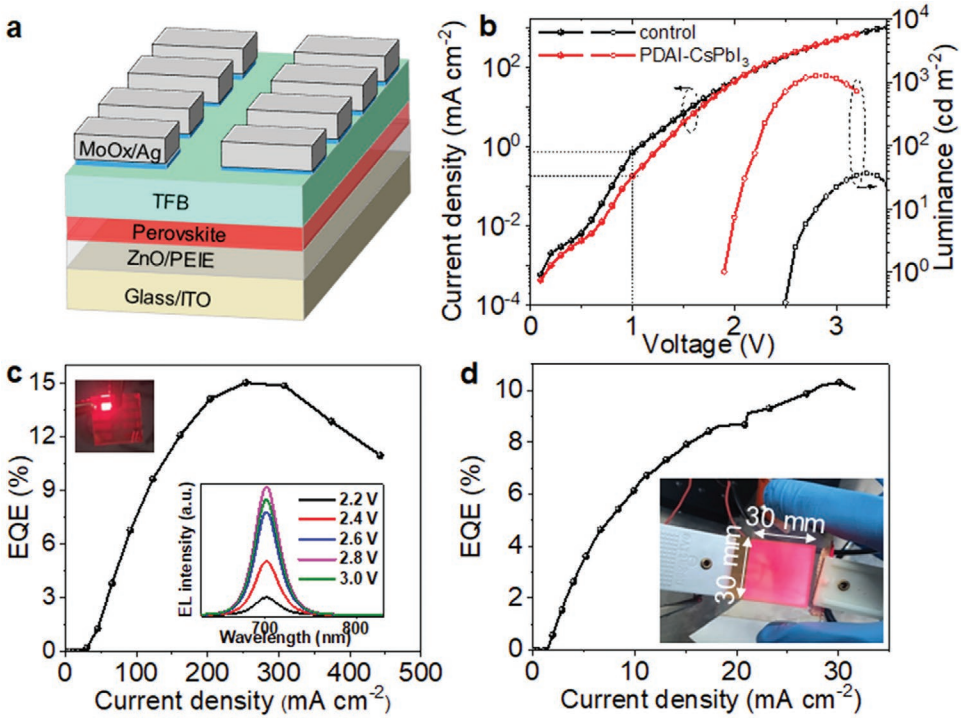

Figure 4. Optoelectronic properties of PeLEDs. a) Illustrated device structure of PeLEDs. b) Current density–voltage–luminance curves of the control PeLED and PDAI-PeLED. c) EQE–current density curve. Image inset: photograph of a working PDAI-PeLED and EL spectra for PDAI-PeLED under different applied voltages. d) EQE–current density curve for large-area PDAI-PeLED. Image inset: photograph of a working large-area PDAI-PeLED.

0.18% (Figure S6, Supporting Information) while the PDAI-$CsPbI_3$-based PeLED (defined as PDAI-PeLED) achieved an impressively high peak EQE of 15.03% with high repeatability (Figure 4b,c and Figure S7, Supporting Information), which is a record efficiency for 3D $CsPbI_3$ PeLEDs to our best knowledge (Table S1, Supporting Information).[19,30,31] To investigate whether the low coverage of PDAI-$CsPbI_3$ film will influence the leakage current, we measured the *J–V* curve of a device without perovskite layer. Figure S8 (Supporting Information) shows that the direct contact of ZnO:PEIE and TFB will not cause serious leakage current. The *J–V* curves of the control PeLED and PDAI-PeLED show that PDAI capping layer can further reduce the leakage current (0.18 mA cm^{-2} for PDAI-PeLED and 0.71 mA cm^{-2} for the control PeLED at 1.0 V, Figure 4b).[45]

PDAI-PeLED can reach a high brightness of 1272 cd m^{-2} with deep-red emission and maintain a high EQE of 14.89% under a current density of 300 mA cm^{-2} which further demonstrates the advantage of 3D $CsPbI_3$-based PeLEDs at high current densities. The peak of electroluminescence (EL) spectra locate at 699 nm with a deep-red chromaticity coordinate of (0.73, 0.27) and the EL spectra keep unchanged under different applied voltages (Figure 4c and Figure S9, Supporting Information). PDAI-PeLED also shows high operation stability and reach a T_{50} lifetime of 1.7 h under a high current density of 100 mA cm^{-2} (Figure S10, Supporting Information).

Our PDAI-assisted one-step method is more attractive for large-area PeLED fabrication because it benefits from an anti-solvent-free process. The PDAI-$CsPbI_3$ precursor film after spin-coating also has wide processing window before annealing treatment which is appreciated for flow-line production.[46] Therefore, we prepared the large-area PDAI-$CsPbI_3$ perovskite film by simply spin-coating the precursor solution directly on the substrate.[47] A large-area PDAI-PeLED with an active area of 9 cm^2 (Figure 4d and Figure S11, Supporting Information) is fabricated, and it can also reach a high EQE of 10.30% and brightness up to 540 cd m^{-2} (Figure S12, Supporting Information). We compared the EQEs of devices with different processing delay times. Figure S13 (Supporting Information) shows that PeLEDs with delay time of 30 min can obtain ≈90% average EQE of the PeLEDs without delay time.

3. Conclusion

We have developed and demonstrated a facile PDAI-assisted method to form 3D γ-$CsPbI_3$ films. PDAI will retard the phase transition rate and in situ form cuboid crystallites. PDAI will further passivate the defects of these cuboid crystallites and significantly improved the PLQY. The PDAI-PeLED can reach a high EQE of 15.03% and T_{50} lifetime of 1.7 h under 100 mA cm^{-2}. This method also shows potential for large-area PeLEDs and commercial production of PeLED modules. Our work suggested that rational molecular modification of 3D $CsPbI_3$ from precursor solution to film formation process can combine the advantages of 3D perovskite with high mobility and cuboid crystallites with reduced trap density.

4. Experimental Section

Materials: CsI and PbI_2 were purchased from Sigma-Aldrich. FAI was purchased Xi'an Polymer Light Technology Corp. DMF was purchased from J&K Scientific Ltd. PDAI was purchased from Macklin.

Device Fabrication: The electron-transport layer (ZnO-PEIE) and hole-transport layer (TFB) were prepared according to a previous report.[48] The concentration for PbI_2 in the perovskite precursor solution was 0.13 M. The perovskite layer was prepared by spin-coating a perovskite precursor solution on ZnO-PEIE/ITO at 4000 rpm for 45 s. The perovskite film was then annealed at 100 °C for 10 min. The top electrode with 7 nm-thickness MoO_x and 60 nm-thickness Ag was prepared by thermal evaporation. The device area for small-area PeLEDs and large-area PeLEDs were 3 mm^2 and 9 cm^2, respectively.

Characterization: The morphology and topology of perovskite films was measured by SEM (JSM-7800F Prime, JEOL) and AFM (MFP-3D, Oxford Instruments), respectively. XRD patterns were obtained by Shimadzu XRD-6100 diffractometer with Cu Kα radiation. NMR was performed using a Bruker AVANCE NEO 600MHz instrument. DLS was carried out using a nanoparticle analyzer (Delsa Nano C, Beckman Coulter). FTIR spectra were collected on Nicolet6700. XPS spectra were measured using an AXIS UltraDLD. ToF-SIMS measurements were made using an ION TOF ToF SIMS 5-100 (area:150 μm × 150 μm), using 30 keV Bi^{3+} primary ion beam with an ion current of 0.43 pA. Steady-state PL, TRPL, and PLQY were measured using an FLS1000 Photoluminescence Spectrometer (Edinburgh Instruments Ltd.) with a 445 nm excitation laser. The *J–V* curves of the PeLEDs were measured uisng a Keithley 2400 source meter (scan rate was 0.1 V s^{-1}). The emitted light from the glass side was collected by an integration sphere coupled with a fiber spectrometer (QE 65 Pro, Ocean Optics).[48]

Supporting Information

Supporting Information is available from the Wiley Online Library or from the author.

Acknowledgements

This work was supported by the NSFC (Grant Nos. 22025505, 51861145101, and 21777096), Program of Shanghai Academic Technology Research Leader (Grant No. 20XD1422200), Cultivating fund of Frontiers Science Center for Transformative Molecules (2019PT02), and China Postdoctoral Science Foundation (2020M671110).

Conflict of Interest

The authors declare no conflict of interest.

Data Availability Statement

Research data are not shared.

Keywords

$CsPbI_3$, cuboid crystallites, deep-red emission, diammonium cations, perovskite light-emitting diodes

Received: July 23, 2021
Revised: August 28, 2021
Published online: October 10, 2021

[1] Q. Dong, Y. Fang, Y. Shao, P. Mulligan, J. Qiu, L. Cao, J. Huang, *Science* **2015**, *347*, 967.
[2] G. Xing, N. Mathews, S. Sun, S. S. Lim, Y. M. Lam, M. Grätzel, S. Mhaisalkar, T. C. Sum, *Science* **2013**, *342*, 344.
[3] S. D. Stranks, V. M. Burlakov, T. Leijtens, J. M. Ball, A. Goriely, H. J. Snaith, *Phys. Rev. Appl.* **2014**, *2*, 034007.
[4] J. Wang, N. Wang, Y. Jin, J. Si, Z. K. Tan, H. Du, L. Cheng, X. Dai, S. Bai, H. He, Z. Ye, M. L. Lai, R. H. Friend, W. Huang, *Adv. Mater.* **2015**, *27*, 2311.
[5] Z. K. Tan, R. S. Moghaddam, M. L. Lai, P. Docampo, R. Higler, F. Deschler, M. Price, A. Sadhanala, L. M. Pazos, D. Credgington, F. Hanusch, T. Bein, H. J. Snaith, R. H. Friend, *Nat. Nanotechnol.* **2014**, *9*, 687.
[6] Z. Xiao, R. A. Kerner, L. Zhao, N. L. Tran, K. M. Lee, T.-W. Koh, G. D. Scholes, B. P. Rand, *Nat. Photonics* **2017**, *11*, 108.
[7] H. Cho, S. H. Jeong, M. H. Park, Y. H. Kim, C. Wolf, C. L. Lee, J. H. Heo, A. Sadhanala, N. Myoung, S. Yoo, S. H. Im, R. H. Friend, T. W. Lee, *Science* **2015**, *350*, 1222.
[8] M. Yuan, L. N. Quan, R. Comin, G. Walters, R. Sabatini, O. Voznyy, S. Hoogland, Y. Zhao, E. M. Beauregard, P. Kanjanaboos, Z. Lu, D. H. Kim, E. H. Sargent, *Nat. Nanotechnol.* **2016**, *11*, 872.
[9] Y. Cao, N. Wang, H. Tian, J. Guo, Y. Wei, H. Chen, Y. Miao, W. Zou, K. Pan, Y. He, H. Cao, Y. Ke, M. Xu, Y. Wang, M. Yang, K. Du, Z. Fu, D. Kong, D. Dai, Y. Jin, G. Li, H. Li, Q. Peng, J. Wang, W. Huang, *Nature* **2018**, *562*, 249.
[10] B. Zhao, S. Bai, V. Kim, R. Lamboll, R. Shivanna, F. Auras, J. M. Richter, L. Yang, L. Dai, M. Alsari, X.-J. She, L. Liang, J. Zhang, S. Lilliu, P. Gao, H. J. Snaith, J. Wang, N. C. Greenham, R. H. Friend, D. Di, *Nat. Photonics* **2018**, *12*, 783.
[11] T. Chiba, Y. Hayashi, H. Ebe, K. Hoshi, J. Sato, S. Sato, Y.-J. Pu, S. Ohisa, J. Kido, *Nat. Photonics* **2018**, *12*, 681.
[12] W. Xu, Q. Hu, S. Bai, C. Bao, Y. Miao, Z. Yuan, T. Borzda, A. J. Barker, E. Tyukalova, Z. Hu, M. Kawecki, H. Wang, Z. Yan, X. Liu, X. Shi, K. Uvdal, M. Fahlman, W. Zhang, M. Duchamp, J.-M. Liu, A. Petrozza, J. Wang, L.-M. Liu, W. Huang, F. Gao, *Nat. Photonics* **2019**, *13*, 418.
[13] Y.-H. Kim, S. Kim, A. Kakekhani, J. Park, J. Park, Y.-H. Lee, H. Xu, S. Nagane, R. B. Wexler, D.-H. Kim, S. H. Jo, L. Martínez-Sarti, P. Tan, A. Sadhanala, G.-S. Park, Y.-W. Kim, B. Hu, H. J. Bolink, S. Yoo, R. H. Friend, A. M. Rappe, T.-W. Lee, *Nat. Photonics* **2021**, *15*, 148.
[14] Y. Dong, Y. K. Wang, F. Yuan, A. Johnston, Y. Liu, D. Ma, M. J. Choi, B. Chen, M. Chekini, S. W. Baek, L. K. Sagar, J. Fan, Y. Hou, M. Wu, S. Lee, B. Sun, S. Hoogland, R. Quintero-Bermudez, H. Ebe, P. Todorovic, F. Dinic, P. Li, H. T. Kung, M. I. Saidaminov, E. Kumacheva, E. Spiecker, L. S. Liao, O. Voznyy, Z. H. Lu, E. H. Sargent, *Nat. Nanotechnol.* **2020**, *15*, 668.
[15] Z. Chen, Z. Li, Z. Chen, R. Xia, G. Zou, L. Chu, S.-J. Su, J. Peng, H.-L. Yip, Y. Cao, *Joule* **2021**, *5*, 456.
[16] Y. Miao, Y. Ke, N. Wang, W. Zou, M. Xu, Y. Cao, Y. Sun, R. Yang, Y. Wang, Y. Tong, W. Xu, L. Zhang, R. Li, J. Li, H. He, Y. Jin, F. Gao, W. Huang, J. Wang, *Nat. Commun.* **2019**, *10*, 3624.
[17] C. Kuang, Z. Hu, Z. Yuan, K. Wen, J. Qing, L. Kobera, S. Abbrent, J. Brus, C. Yin, H. Wang, W. Xu, J. Wang, S. Bai, F. Gao, *Joule* **2021**, *5*, 618.
[18] Y. Guo, S. Apergi, N. Li, M. Chen, C. Yin, Z. Yuan, F. Gao, F. Xie, G. Brocks, S. Tao, N. Zhao, *Nat. Commun.* **2021**, *12*, 644.
[19] C. Yi, C. Liu, K. Wen, X. K. Liu, H. Zhang, Y. Yu, N. Fan, F. Ji, C. Kuang, B. Ma, C. Tu, Y. Zhang, C. Xue, R. Li, F. Gao, W. Huang, J. Wang, *Nat. Commun.* **2020**, *11*, 4736.
[20] Z. Chu, Q. Ye, Y. Zhao, F. Ma, Z. Yin, X. Zhang, J. You, *Adv. Mater.* **2021**, *33*, 2007169.
[21] S. Zhang, C. Yi, N. Wang, Y. Sun, W. Zou, Y. Wei, Y. Cao, Y. Miao, R. Li, Y. Yin, N. Zhao, J. Wang, W. Huang, *Adv. Mater.* **2017**, *29*, 1606600.
[22] H. Li, H. Lin, D. Ouyang, C. Yao, C. Li, J. Sun, Y. Song, Y. Wang, Y. Yan, Y. Wang, Q. Dong, W. C. H. Choy, *Adv. Mater.* **2021**, *33*, 2008820.
[23] G. E. Eperon, G. M. Paternò, R. J. Sutton, A. Zampetti, A. A. Haghighirad, F. Cacialli, H. J. Snaith, *J. Mater. Chem. A* **2015**, *3*, 19688.
[24] J. A. Steele, H. Jin, I. Dovgaliuk, R. F. Berger, T. Braeckevelt, H. Yuan, C. Martin, E. Solano, K. Lejaeghere, S. M. J. Rogge, C. Notebaert, W. Vandezande, K. P. F. Janssen, B. Goderis, E. Debroye, Y.-K. Wang, Y. Dong, D. Ma, M. Saidaminov, H. Tan, Z. Lu, V. Dyadkin, D. Chernyshov, V. Van Speybroeck, E. H. Sargent, J. Hofkens, M. B. J. Roeffaers, *Science* **2019**, *365*, 679.
[25] J. Si, Y. Liu, Z. He, H. Du, K. Du, D. Chen, J. Li, M. Xu, H. Tian, H. He, D. Di, C. Lin, Y. Cheng, J. Wang, Y. Jin, *ACS Nano* **2017**, *11*, 11100.
[26] J. Pan, Y. Shang, J. Yin, M. De Bastiani, W. Peng, I. Dursun, L. Sinatra, A. M. El-Zohry, M. N. Hedhili, A. H. Emwas, O. F. Mohammed, Z. Ning, O. M. Bakr, *J. Am. Chem. Soc.* **2018**, *140*, 562.
[27] J. S. Yao, J. Ge, K. H. Wang, G. Zhang, B. S. Zhu, C. Chen, Q. Zhang, Y. Luo, S. H. Yu, H. B. Yao, *J. Am. Chem. Soc.* **2019**, *141*, 2069.
[28] X. Shen, Y. Zhang, S. V. Kershaw, T. Li, C. Wang, X. Zhang, W. Wang, D. Li, Y. Wang, M. Lu, L. Zhang, C. Sun, D. Zhao, G. Qin, X. Bai, W. W. Yu, A. L. Rogach, *Nano Lett.* **2019**, *19*, 1552.
[29] A. Swarnkar, A. R. Marshall, E. M. Sanehira, B. D. Chernomordik, D. T. Moore, J. A. Christians, T. Chakrabarti, J. M. Luther, *Science* **2016**, *354*, 92.
[30] B. Han, B. Cai, Q. Shan, J. Song, J. Li, F. Zhang, J. Chen, T. Fang, Q. Ji, X. Xu, H. Zeng, *Adv. Funct. Mater.* **2018**, *28*, 1804285.
[31] Y. Ke, N. Wang, D. Kong, Y. Cao, Y. He, L. Zhu, Y. Wang, C. Xue, Q. Peng, F. Gao, W. Huang, J. Wang, *J. Phys. Chem. Lett.* **2019**, *10*, 380.
[32] Y. Wang, M. I. Dar, L. K. Ono, T. Zhang, M. Kan, Y. Li, L. Zhang, X. Wang, Y. Yang, X. Gao, Y. Qi, M. Gratzel, Y. Zhao, *Science* **2019**, *365*, 591.
[33] T. Zhang, Y. Wang, X. Wang, M. Wu, W. Liu, Y. Zhao, *Sci. Bull.* **2019**, *64*, 1773.
[34] H. Cho, Y. H. Kim, C. Wolf, H. D. Lee, T. W. Lee, *Adv. Mater.* **2018**, *30*, 1704587.
[35] Z. Yuan, Y. Miao, Z. Hu, W. Xu, C. Kuang, K. Pan, P. Liu, J. Lai, B. Sun, J. Wang, S. Bai, F. Gao, *Nat. Commun.* **2019**, *10*, 2818.
[36] A. Marronnier, G. Roma, S. Boyer-Richard, L. Pedesseau, J. M. Jancu, Y. Bonnassieux, C. Katan, C. C. Stoumpos, M. G. Kanatzidis, J. Even, *ACS Nano* **2018**, *12*, 3477.
[37] Y. Wang, X. Liu, T. Zhang, X. Wang, M. Kan, J. Shi, Y. Zhao, *Angew. Chem., Int. Ed.* **2019**, *58*, 16691.
[38] Y. Xu, W. Xu, Z. Hu, J. A. Steele, Y. Wang, R. Zhang, G. Zheng, X. Li, H. Wang, X. Zhang, E. Solano, M. B. J. Roeffaers, K. Uvdal, J. Qing, W. Zhang, F. Gao, *J. Phys. Chem. Lett.* **2021**, *12*, 5836.
[39] X. Wang, Y. Fan, L. Wang, C. Chen, Z. Li, R. Liu, H. Meng, Z. Shao, X. Du, H. Zhang, G. Cui, S. Pang, *Chem* **2020**, *6*, 1369.
[40] M. Hadadian, J. P. Correa-Baena, E. K. Goharshadi, A. Ummadisingu, J. Y. Seo, J. Luo, S. Gholipour, S. M. Zakeeruddin, M. Saliba, A. Abate, M. Gratzel, A. Hagfeldt, *Adv. Mater.* **2016**, *28*, 8681.
[41] Z. Yang, W. Zhang, S. Wu, H. Zhu, Z. Liu, Z. Liu, Z. Jiang, R. Chen, J. Zhou, Q. Lu, Z. Xiao, L. Shi, H. Chen, L. K. Ono, S. Zhang, Y. Zhang, Y. Qi, L. Han, W. Chen, *Sci. Adv.* **2021**, *7*, eabg3749.
[42] L. Zhu, H. Cao, C. Xue, H. Zhang, M. Qin, J. Wang, K. Wen, Z. Fu, T. Jiang, L. Xu, Y. Zhang, Y. Cao, C. Tu, J. Zhang, D. Liu, G. Zhang, D. Kong, N. Fan, G. Li, C. Yi, Q. Peng, J. Chang, X. Lu, N. Wang, W. Huang, J. Wang, *Nat. Commun.* **2021**, *12*, 5081.

[43] Y. Zou, P. Teng, W. Xu, G. Zheng, W. Lin, J. Yin, L. Kobera, S. Abbrent, X. Li, J. A. Steele, E. Solano, M. B. J. Roeffaers, J. Li, L. Cai, C. Kuang, I. G. Scheblykin, J. Brus, K. Zheng, Y. Yang, O. F. Mohammed, O. M. Bakr, T. Pullerits, S. Bai, B. Sun, F. Gao, *Nat. Commun.* **2021**, *12*, 4831.

[44] D. Di, K. P. Musselman, G. Li, A. Sadhanala, Y. Ievskaya, Q. Song, Z. K. Tan, M. L. Lai, J. L. MacManus-Driscoll, N. C. Greenham, R. H. Friend, *J. Phys. Chem. Lett.* **2015**, *6*, 446.

[45] X. K. Liu, W. Xu, S. Bai, Y. Jin, J. Wang, R. H. Friend, F. Gao, *Nat. Mater.* **2021**, *20*, 10.

[46] M. Yang, Z. Li, M. O. Reese, O. G. Reid, D. H. Kim, S. Siol, T. R. Klein, Y. Yan, J. J. Berry, M. F. A. M. van Hest, K. Zhu, *Nat. Energy* **2017**, *2*, 17038.

[47] S. Chu, W. Chen, Z. Fang, X. Xiao, Y. Liu, J. Chen, J. Huang, Z. Xiao, *Nat. Commun.* **2021**, *12*, 147.

[48] N. Wang, L. Cheng, R. Ge, S. Zhang, Y. Miao, W. Zou, C. Yi, Y. Sun, Y. Cao, R. Yang, Y. Wei, Q. Guo, Y. Ke, M. Yu, Y. Jin, Y. Liu, Q. Ding, D. Di, L . Yang, G. Xing, H. Tian, C. Jin, F. Gao, R. H. Friend, J. Wang, W. Huang, *Nat. Photonics* **2016**, *10*, 699.